RESEARCH ARTICLE

Key Points:
- Airborne observed dry layers in the tropical troposphere are well represented in GFS analyses
- GFS global climatology shows strong connection between dry layers and subtropical jet
- Ubiquitous dry, ozone-rich air is a signature of extratropical UTLS influence in subtropics

Dry layers in the tropical troposphere observed during CONTRAST and global behavior from GFS analyses
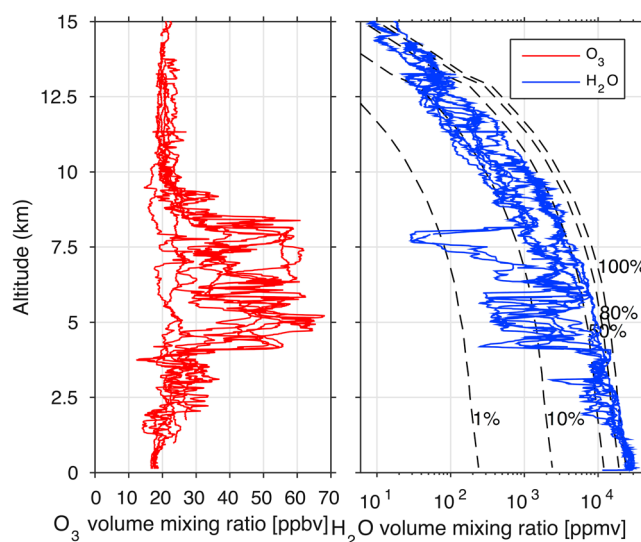
William J. Randel[1], Louis Rivoire[2], Laura L. Pan[1], and Shawn B. Honomichl[1]

[1]National Center for Atmospheric Research, Boulder, Colorado, USA, [2]Department of Atmospheric Sciences, Colorado State University, Fort Collins, Colorado, USA

Abstract The Convective Transport of Active Species in the Tropics (CONTRAST) experiment was an aircraft-based field campaign conducted from Guam (14°N, 145°E) during January–February 2014. Aircraft measurements included over 80 vertical profiles from the boundary layer to the upper troposphere (~15 km). A large fraction of these profiles revealed layered structures with very low water vapor (relative humidity <20%) and enhanced ozone, primarily in the lower-middle troposphere (~3–9 km). Comparing CONTRAST water vapor measurements with co-located profiles from National Centers for Environmental Prediction Global Forecast System (GFS) analyses, we find good agreement for dry layers, including profile-by-profile comparisons and statistical behavior. We then utilize GFS data to evaluate the frequency of occurrence and 3-D structure of dry layers for the CONTRAST period to provide perspective to the campaign measurements and evaluate the global climatological behavior based on a longer record. GFS data show that dry layers occur ~50–80% of the time in the subtropical troposphere, maximizing on the equatorward side of the subtropical jets in the winter hemisphere. Subtropical dry layers occur most frequently over isentropic levels ~320–340 K, which extend into the extratropical upper troposphere-lower stratosphere (UTLS). Similar statistical behavior of dry, ozone-rich layers is found in long-term balloon measurements from Reunion Island (21°S, 56°E). The climatologically frequent occurrence of dry, ozone-rich layers, plus their vertical and spatial structures linked to the subtropical jets, all suggest that dry layers are linked to quasi-isentropic transport from the extratropical UTLS and suggest a ubiquitous UTLS influence on the subtropical middle troposphere.

1. Introduction

Dry regions in the subtropical troposphere are a climatological feature that has a strong impact on global radiative balances, as they influence the ability of the climate system to radiate heat to space [*Pierrehumbert*, 1995]. Satellite observations show that dry regions (areas with relative humidity (RH) less than 20%) occur as a climatological feature in the lower-middle troposphere, centered near 20–30°N and 20–30°S [e.g., *Gettelman et al.*, 2006; *Ruzmaikin et al.*, 2014]. The mechanisms that maintain these dry regions are complex and are linked to some combination of quasi-isentropic transport from the extratropical upper troposphere-lower stratosphere (UTLS) and downward circulation in the Hadley cells. *Galewsky et al.* [2005] used trajectory calculations based on meteorological reanalysis to demonstrate that dry air in the subtropical troposphere is produced by isentropic transport of dry air by midlatitude eddies. Similar conclusions were reached by *Cau et al.* [2007], who furthermore describe different dynamical mechanisms for exchanges with the extratropical UTLS. *Dessler and Minschwaner* [2007] highlight the importance of isentropic exchanges with midlatitudes, in addition to downward fluxes from the upper troposphere in the Hadley circulation. A recent review and discussion of the dry subtropical regions is found in *Sherwood et al.* [2009].

A phenomenon possibly related to the climatologically dry subtropics is the frequent occurrence of isolated dry layers throughout the tropical and subtropical troposphere, which have been observed in radiosonde and aircraft measurements during research campaigns. Observations during the early 1990s from Central Equatorial Pacific Experiment [*Kley et al.*, 1997] and Tropical Ocean–Global Atmosphere Coupled Ocean-Atmosphere Response Experiment [*Mapes and Zuidema*, 1996; *Yoneyama and Parsons*, 1999] noted dry, narrow vertical layers in the deep tropics and highlighted their influence on thermodynamic and radiative structures. Aircraft measurements from the series of NASA Pacific Exploratory Mission (PEM) experiments (PEM-West A,B and PEM-Tropics A,B [*Newell et al.*, 1996; *Wu et al.*, 1997; *Stoller et al.*, 1999; *Thouret et al.*, 2001]) showed the frequent occurrence of layered structures in water vapor and ozone (and other

Figure 1. Vertical profiles of (left) ozone and (right) water vapor mixing ratios from CONTRAST research flight number 3 (23 January 2014). The water vapor mixing ratio is on a log scale, and the dashed lines indicate the isopleths of relative humidity.

constituents) in the tropics. The most frequently occurring structures were layers with anomalously dry air and high ozone. The frequent occurrence of such layers was furthermore documented using Measurements of Ozone and Water Vapor by Airbus In-Service Aircraft (MOZAIC) aircraft measurements, in particular using profiles on takeoff and landing, by *Thouret et al.* [2000]. This overall behavior from the PEM and MOZAIC aircraft data were summarized by *Newell et al.* [1999], showing that approximately 15–20% of the tropical atmosphere up to 12 km were occupied by layered structures (with maximum occurrence near 5–7 km); the layers were typically 0.5–1.0 km thick, and approximately 50% of the observed layers were anomalously dry with enhanced ozone. A complementary observational study by *Hayashi et al.* [2008] highlighted the frequent occurrence of tropospheric ozone-rich layers in tropical ozonesonde measurements, finding that 50–80% of the events were coincident with extreme dry layers. *Kley et al.* [2007] also show measurements of dry, high-ozone air in the subtropical latitudes of the central Atlantic Ocean, surrounding wet, low-ozone air over the convective deep tropics.

The Convective Transport of Active Species in the Tropics (CONTRAST) experiment was an aircraft-based field campaign conducted from Guam (14°N, 145°E) during January–February 2014, using the NSF/National Center for Atmospheric Research (NCAR) Gulfstream V (GV) research aircraft [*Pan et al.*, 2016]. CONTRAST was one of three coordinated airborne experiments, aimed at investigating the impact of deep convection and convective transport on atmospheric composition over the tropical western Pacific (TWP) Ocean during boreal winter. A total of 16 research flights were conducted during CONTRAST using the GV, with highly accurate measurements of water vapor and a large suite of chemical tracers, in addition to meteorological parameters. Each of the research flights included long horizontal legs (typically between 12 and 14 km), in addition to several vertical profiles from the marine boundary layer (near 0.1 km) to the upper troposphere (up to ~15 km). Including sampling during takeoff and landing, there were over 80 vertical profiles obtained over the TWP during CONTRAST. A majority of the vertical profiles from CONTRAST showed layered structures with low water vapor and enhanced ozone, primarily over altitudes of 3–9 km (approximately 320 K to 340 K in potential temperature). An example of this behavior is shown in Figure 1 for profiles during the research flight of 23 January 2014. The measurements show extremely dry air in horizontal layered structures over 4–8 km, with values as low as 30 ppmv (RH <1%) near 8 km. The dry layers in Figure 1 have sharp vertical gradients and are strongly correlated with enhanced ozone. Such anomalously dry, ozone-rich layers were observed in ~80% of the profiles during CONTRAST. While the dry, ozone-rich layers in CONTRAST are similar to previous observations in the tropics noted above, the frequency of occurrence is much higher than previous measurements (e.g., *Newell et al.* [1999] and *Thouret et al.* [2000] calculate occurrence frequencies of 15–20%). Furthermore, the thickness of the layers from CONTRAST is often several kilometers (up to ~7 km), much wider than the layers of ~0.5–1.0 km reported in other studies (although the specific definition of a "layer" can vary among different studies).

The goal of this study is to utilize global analyses of water vapor from a state-of-the-art meteorological analysis system to compare with CONTRAST measurements and to provide a broader perspective and context to the relatively short-term field experiment. We use analyses from the National Centers for Environmental Prediction (NCEP) Global Forecast System (GFS), as these fields were part of the meteorological products utilized in CONTRAST. We explicitly compare the water vapor profiles measured in CONTRAST with nearly

co-located GFS results. The comparisons show good agreement, demonstrating that the dry layers are reasonably well captured in the GFS results. We then use the globally gridded GFS analyses to quantify the large-scale behavior of dry layers during CONTRAST and additionally use a longer-term record to evaluate the climatological behavior of anomalously dry layers over the globe.

The GFS data show that dry layers are a common feature in the subtropics, especially in the winter hemisphere. We present further analyses of a long record of balloon measurements of water vapor and ozone from Reunion Island (21°S, 56°E), which is located within a maximum dry layer occurrence region identified by the GFS analyses. The Reunion Island observations are compared with the CONTRAST and GFS results and further characterize the dry, ozone-rich layers in the subtropical troposphere. The consistency of the GFS, CONTRAST, and balloon sounding data, plus the geographical and season locations of the dry air derived from GFS data, provide information on the mechanisms maintaining the subtropical dry regions.

As a note, our discussions often involve the terms tropics, subtropics, and extratropics. While there are various definitions of these regions based on different metrics (see the discussion in *Birner et al.* [2014]), in this work we refer to the region 20° equatorward of the subtropical jet core (zonal wind maximum) to be subtropics. This choice assigns the subtropics in the winter hemisphere, where we identify the more frequent dry layers, to be approximately 10°–30° in latitude. Correspondingly, we refer to the region equatorward of the subtropics, approximately 10°S–10°N, as the deep tropics, and poleward of the jet core to be the extratropics.

2. Data and Analyses

2.1. CONTRAST Observations

An overview of the CONTRAST field experiment is provided in *Pan et al.* [2016]. During the CONTRAST campaign time period (January–February 2014), the base of the flight operations (Guam) is located in the descending branch of the Hadley cell, with only occasional deep convection. The region south of Guam is dominated by active convection. Most flights were conducted south of Guam, over the tropical Pacific warm pool, since the campaign was designed to target the convective influence on the upper troposphere. Satellite measurements from CloudSat show that upper troposphere cloud fractions are approximately 20–30% in the region south of Guam [*Pan et al.*, 2016, Figure 3].
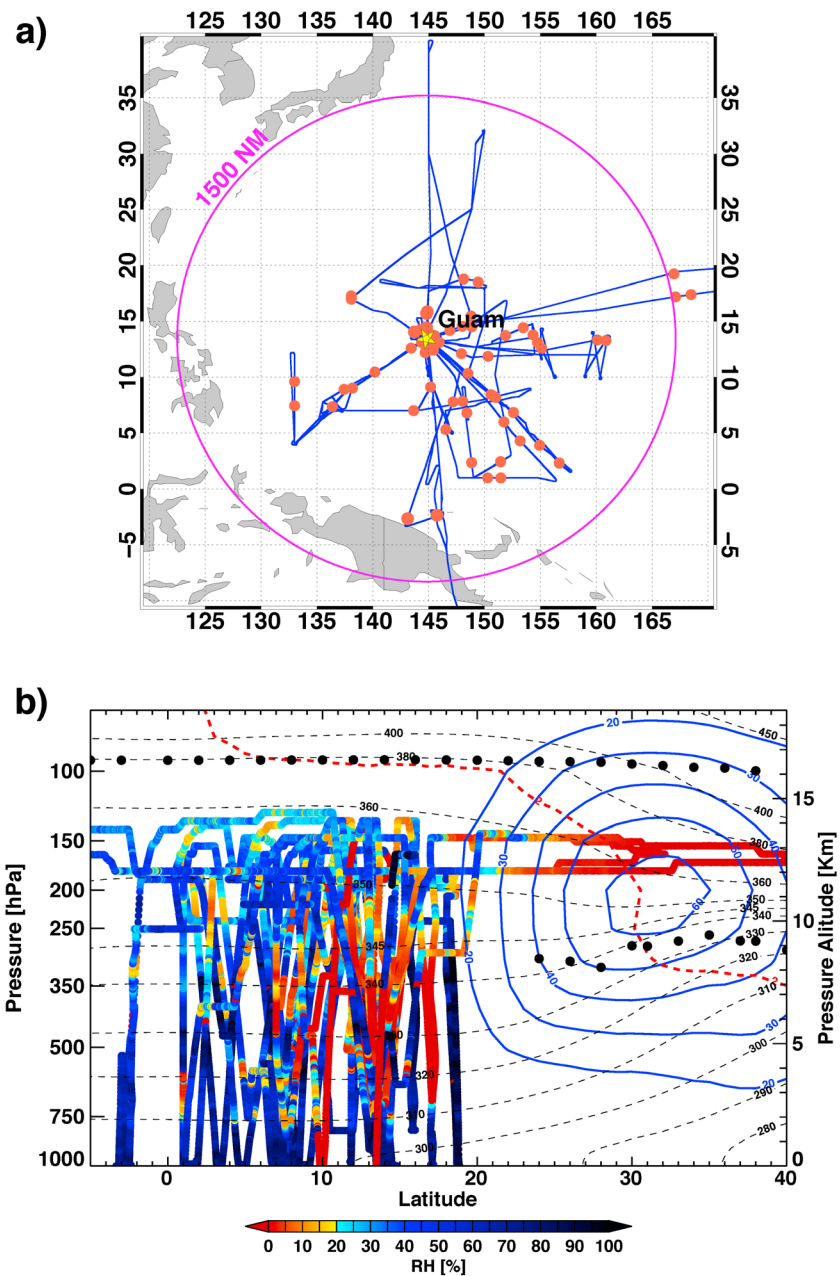
The in situ water vapor measurements on the GV were made using the vertical cavity surface-emitting laser instrument [*Zondlo et al.*, 2010]. The accuracy of water vapor mixing ratio is estimated to be within 6% for the range of measurements during CONTRAST. Relative humidity (RH) is calculated from the water vapor measurements and co-located GV temperatures [*Pan et al.*, 2015]; RH is calculated with respect to liquid water (ice) for temperatures above (below) 0°C. In situ ozone measurements were made using the NCAR chemiluminesence instrument [*Ridley et al.*, 1992], with an accuracy estimated within 5%. Data for the CONTRAST experiment are reported at 1 Hz. With typical airspeed and vertical climb rates, the vertical resolution for profiles at 1 Hz sampling is approximately 7 m.

The flight tracks for the CONTRAST campaign are illustrated in Figure 2a, together with locations of the vertical profiles. Values of RH along the flight tracks are shown in Figure 2b, highlighting the frequent occurrence and broad spatial extent of the dry layers (RH <20%) encountered throughout the experiment.

As noted above, the dry layers in CONTRAST were almost always observed in combination with enhanced ozone (values of 40–80 ppbv, well above the background of ~20 ppbv; Figure 1). *Pan et al.* [2015] analyzed the behavior of the enhanced ozone layers, including their close association with coincident dry layers. The spatial patterns of enhanced ozone [*Pan et al.*, 2016, Figure 11] are similar to the dry layers in Figure 2b. The statistical relationship of water vapor (expressed as RH) and ozone for the CONTRAST vertical profiles in the lower-middle troposphere is shown in Figure 3. The distribution is organized into two distinct groups of air characteristics: extremely dry air (RH <10–20%) with ozone above 30 ppbv and moister air (RH >40%) with ozone ~20 ppbv. The overall distribution may be characterized as bimodal in either ozone [*Pan et al.*, 2015] or RH separately, but the two-dimensional ozone-RH distribution clearly identifies this behavior, serving as a fingerprint for the dry, high-ozone layers.
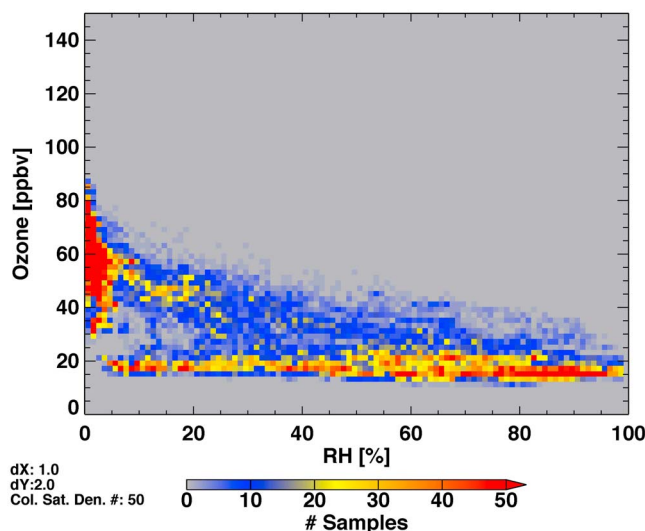
2.2. GFS Analyses

The NCEP GFS is a comprehensive weather analysis forecast model described in http://www.emc.ncep.noaa.gov/GFS/.php. Our focus is on the GFS analysis of water vapor (or RH, derived from combined water vapor

Figure 2. (a) Map showing CONTRAST research flights, with red dots indicating locations of vertical profiles from near-surface to the upper troposphere. (b) Flight tracks from CONTRAST color coded according to relative humidity. The background lines indicate the zonal winds (blue), isentropes (black dashed), PV = 2 tropopause (red dashed line), and thermal tropopause (black dots) near longitude 145°E.

and temperature fields), sampled 4 times daily on a horizontal grid of 0.5° × 0.5°, and standard pressure levels (with approximately 1 km vertical spacing). Some of the important observational data that help to constrain the humidity analyses include high vertical resolution water vapor measurements from Atmospheric Infrared Sounder (AIRS) [*Ruzmaikin et al.*, 2014] and Infrared Atmospheric Sounding Interferometer (IASI) [e.g., *Hilton et al.*, 2009] satellite instruments, which are incorporated into an assimilation system with high-quality meteorological forecasts. *Ciesielski et al.* [2014] compare GFS analyses of RH with high-quality radiosonde RH measurements in the tropics, showing reasonable agreement over most of the troposphere but a moist bias in the upper troposphere (pressures <300 hPa).

Figure 3. Two-dimensional distribution of ozone versus relative humidity for all of the CONTRAST vertical profiles, based on measurements over altitudes 3–9 km (the region of most frequent dry layers).

2.3. Reunion Island Balloon Soundings

Regular ozonesonde measurements have been made at Reunion Island (21°S, 56°E) as part of the Southern Hemisphere Additional Ozonesondes program since 1998 [*Thompson et al.*, 2003]. Soundings are available approximately 1–4 times per month, with a total of over 500 soundings during 1998–2015. Balloon sondes typically extend from the surface to ~30 km or above. Ozone data are from electrochemical concentration cell measurements, with a precision (accuracy) better than ±3–5% (±5–10%) below 30 km [*Smit et al.*, 2007]. Temperature, pressure, and humidity are obtained from Vaisala RS80 radiosondes during 1998–2006 and French Modem radio-

sondes after 2007. Because of relatively large uncertainties (and dry biases) for the radiosonde humidity measurements above 10 km [*Miloshevich et al.*, 2006], we focus on the radiosonde humidity measurements over 0–10 km. *Ciesielski et al.* [2014] report moist biases of ~10% in the Modem radiosondes for altitudes up to 10 km, but these relatively small biases should not strongly influence the results shown here.
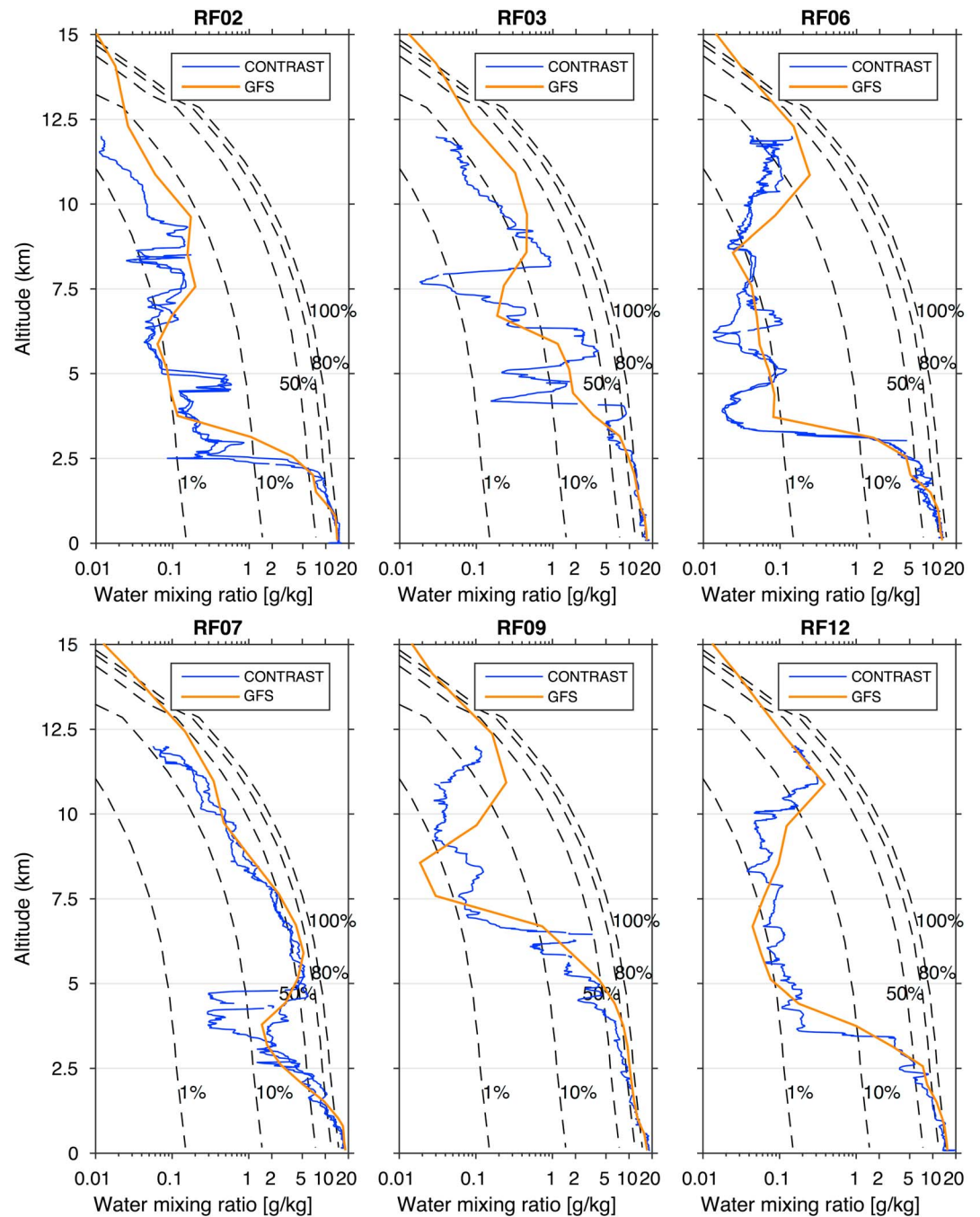
3. Results

3.1. Comparison of CONTRAST In Situ Water Vapor with GFS Analyses

We have compared the aircraft in situ water vapor profiles with nearly co-located GFS analyses for all of the 80 vertical profiles during CONTRAST. Figure 4 shows the examples for six profiles with anomalously dry layers during separate research flights (hereafter, "dry layers" are defined as regions with RH <20%). The dry layers in these profiles have a range of behaviors, from broad layers approximately 5–7 km thick (on research flights RF02, RF06, RF09, and RF12) to relatively narrow layers 1–2 km thick (RF03 and RF07). In general, broader layers were observed in the subtropics and narrower layers in the deep tropics. For comparison, we show the GFS analysis results for each profile interpolated from nearby grid points, using the analysis closest in time to each research flight. Overall the GFS analyses are in reasonable agreement with the in situ measurements for each comparison, especially for the broader vertical-scale features. The extreme dryness of the narrow features on RF03 and RF07 is not accurately captured in the analyses, although the altitude of the layers is reasonably correct. Another difference between GFS and CONTRAST measurements is the sharpness of the vertical gradients at the edges of the layers, which GFS cannot reproduce because of its vertical resolution. Comparisons as in Figure 4 were examined for all of the CONTRAST profiles, revealing only a few cases (~10%) where the overall profiles were in poor agreement.

Figures 5a and 5b show the scatterplots of GFS versus CONTRAST humidity observations combining all of the 80 vertical profiles, comparing specific humidity (Figure 5a) and relative humidity (Figure 5b). Results in Figure 5 focus on altitudes 3–9 km (the region of most frequent dry layers). In these plots we have smoothed the high-resolution CONTRAST measurements by taking 60 s averages along the flight tracks (separately for water vapor and temperature). This results in an approximate vertical smoothing over ~0.5 km, providing more comparable vertical resolution between GFS and CONTRAST. Specific humidity comparisons (Figure 5a) show strong correlations (r^2 ~0.95, calculated in log coordinates because of the large range of variability), although much of the overall structure is tied to the general decrease of water vapor with altitude. The direct comparisons show excellent agreement for relatively high values of specific humidity (>1 g/kg), while for lower values the GFS analyses show a systematic wet bias (more than a factor of 2 for specific humidity <0.1 g/kg). A more stringent comparison is given by comparing point-by-point values of RH (Figure 5b).
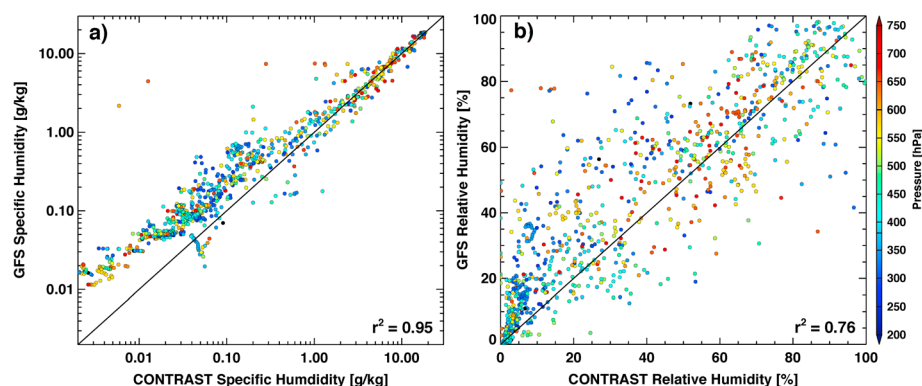
Figure 4. Vertical profiles of water vapor mixing ratio from CONTRAST (blue lines) and co-located GFS analyses (orange), for measurements from six separate research flights. Note the log horizontal axes. The black dashed lines indicate the isopleths of relative humidity.
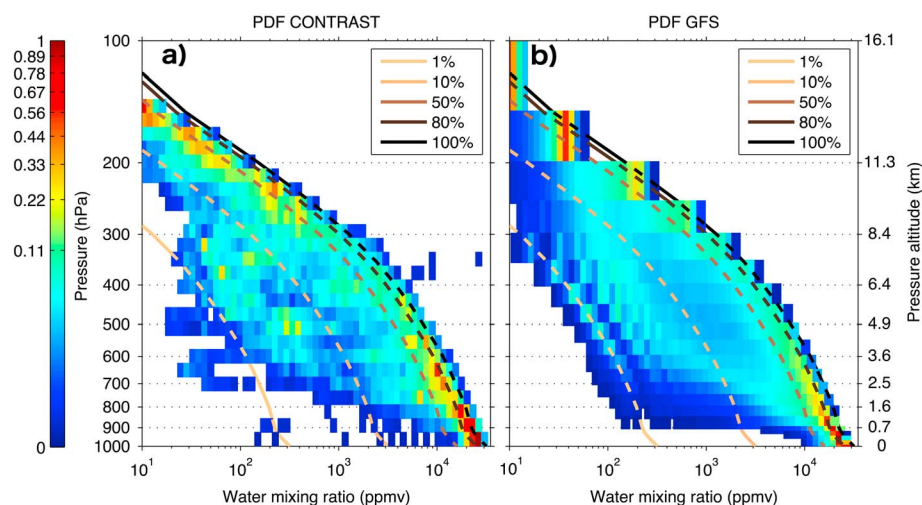
The results show strong correlation (r^2 ~0.76) but also show a moist bias for the GFS analysis. The driest air masses in CONTRAST (RH <10%) do correspond to dry air in GFS analyses, although slightly moister (RH <20%). However, the overall comparisons in Figure 5 suggest that relatively dry and moist regions observed in CONTRAST are captured in the GFS analyses (and a threshold of RH <20% will capture the driest air in both data sets).

Further comparisons of the in situ and GFS data are made by evaluating probability distribution functions of water vapor mixing ratio versus altitude, as shown in Figure 6. Results from the in situ measurements
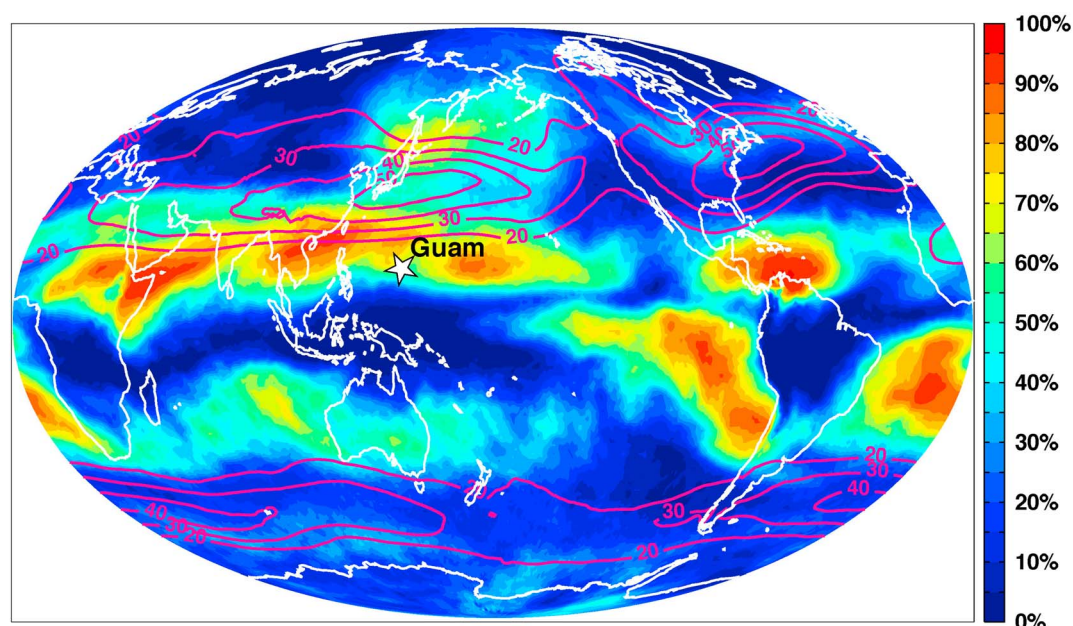
Figure 5. Scatterplots of CONTRAST water vapor measurements versus co-located GFS analyses for (a) specific humidity (note the logarithmic axes) and (b) relative humidity. Results are based on all of the 80 vertical profiles during CONTRAST. The in situ CONTRAST water vapor and temperature measurements are averaged in time using 60 s averages to make these comparisons, corresponding to an approximate vertical averaging of ~0.5 km.

(Figure 6a) are based on the 80 individual vertical profiles, organized into 0.5 km altitude bins, with the distribution normalized for each separate altitude. The results in Figure 6a highlight the frequent occurrence of dry air over altitudes 3–9 km, with RH often below 10%. Results from GFS data (Figure 6b) are calculated in a similar manner but include all grid points in the CONTRAST domain (0–20°N, 130–165°E; see Figure 2a) for all days during January–February 2014. These plots thus compare the statistical distribution from the actual CONTRAST flight sampling versus the GFS analysis over a similar domain (with much denser space-time sampling). The statistical behavior of GFS data in Figure 6b shows quite reasonable agreement to the CONTRAST results, showing the frequent occurrence of dry air over a similar altitude range (3–9 km). Overall these comparisons of individual profiles (Figure 4), statistics of all profiles (Figure 5), and statistics for the region around Guam (Figure 6) show good agreement between in situ measurements from CONTRAST and GFS analyses. Although there is a systematic wet bias in the GFS analyses for the driest air masses (Figure 5), the GFS data are able to capture the overall behavior of the extreme dry air. This prompts the use of GFS data to evaluate the behavior of dry air over larger geographic areas, as a context for the CONTRAST measurements.

Figure 6. Distribution of water vapor mixing ratios as a function of altitude for (a) CONTRAST measurements and (b) GFS analyses. The CONTRAST data are from all of the vertical profiles, binned into 0.5 km altitude levels. The GFS analyses are sampled over a region around Guam (0–20°N, 130–165°E) for the time period covering CONTRAST and are on the standard pressure levels. The distributions are normalized for each separate vertical level. The heavy dashed lines indicate the isopleths of relative humidity.

Figure 7. Spatial distribution of the occurrence frequency of dry air (RH <20%) at the 330 K isentropic level for statistics during January–February 2014 (during CONTRAST), derived from GFS analyses. The pink lines show the corresponding zonal winds (m/s). The location of Guam is noted.

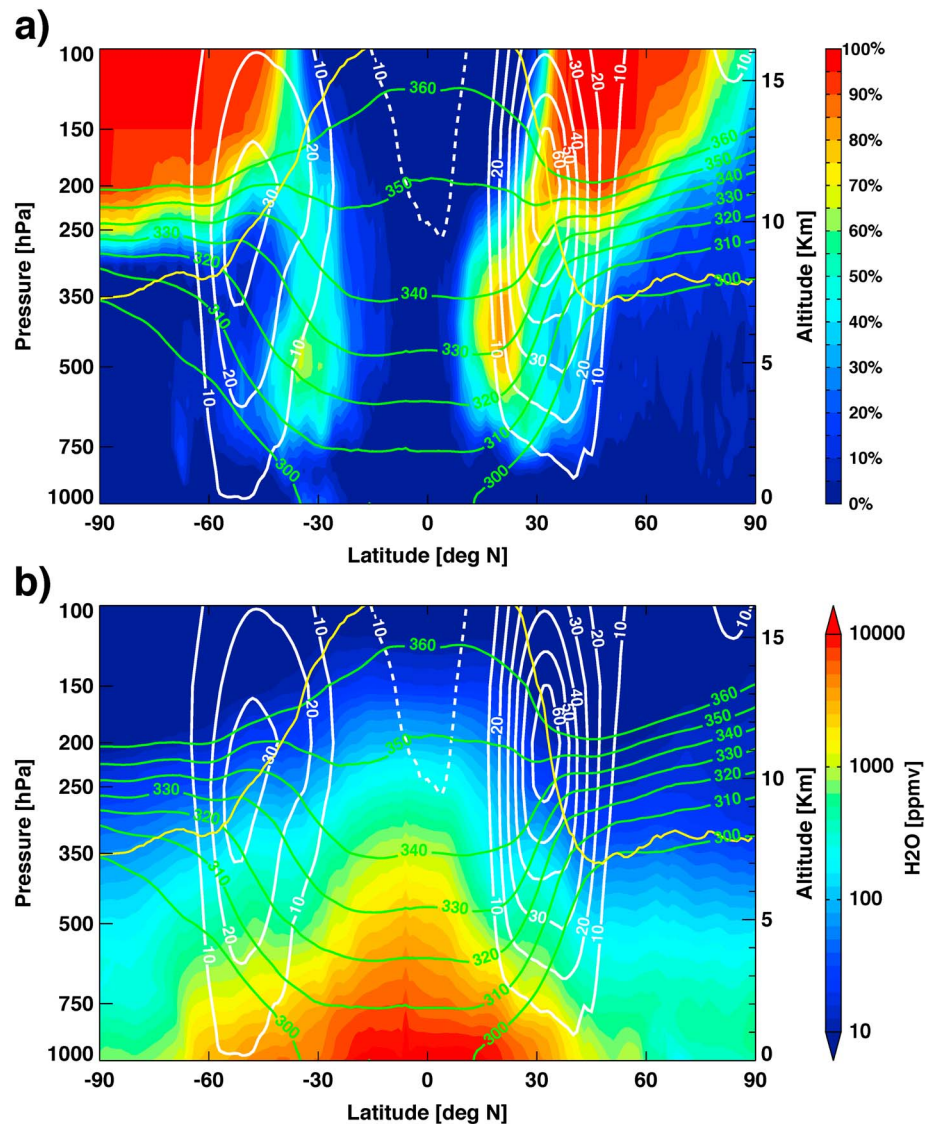### 3.2. GFS Distribution of Dry Air During CONTRAST

Here we use the gridded GFS analysis to identify the frequency and spatial structure of the dry layers during the CONTRAST period to give a large-scale perspective to the aircraft measurements. The frequency of occurrence of dry air (RH <20%) on the 330 K isentropic level, based on GFS data during January–February 2014, is shown in Figure 7. Here we simply count the occurrence of dry air at each grid point and calculate a fractional occurrence. In the deep tropics the 330 K isentrope is near 5.5 km (~500 hPa), which is near the level of maximum occurrence of dry air in Figure 6; this isentrope slopes to higher altitudes (~10–11 km) in middle latitudes (see Figure 2b). The results based on GFS data in Figure 7 show that dry air occurs frequently (above 60–70% of the time) in the subtropical region near Guam (~10–30°N), over longitudes ~100–200°E, with maximum occurrence on the equatorward side of the subtropical jet. Dry regions occur frequently over other isolated regions in the tropics in Figure 7, but the most extensive regions of dry air occur in the northern subtropics near Guam.

Figure 8a shows a latitude-height cross section of the dry air occurrence frequency from GFS data at longitude 145°E, which is near the maximum identified in Figure 7 (and close to Guam). Figure 8a includes the isentropes and zonal winds to provide a large-scale dynamical perspective. The patterns in Figure 8a show the enhanced occurrence frequency in the northern subtropics (over ~10–30°N), spanning isentropic levels ~320–340 K (altitudes 3–9 km). These maxima occur on the equatorward side of the time mean subtropical jet near 35°N. There are weaker frequency maxima (~40%) in the southern subtropics, which are similarly positioned on the equatorward side of the jet centered near 45°S. There are also frequent low-RH dry regions in the middle- and high-latitude stratosphere in both hemispheres in Figure 8a, as expected. For comparison, Figure 8b shows the time-averaged water vapor mixing ratio from GFS data at the same longitude, highlighting the moist tropics and lower troposphere in middle latitudes, with strong latitudinal gradients along isentropes that span the tropics to midlatitudes and cross beneath the subtropical jet core (e.g., 320–340 K). The high frequency of subtropical dry air in Figure 8a occurs in this region of strong gradients, which separate the moist tropics from relatively dry air in the extratropics.

3.3. Climatology of Subtropical Dry Air

The GFS data allow the calculation of the space-time behavior of dry air occurrence frequency throughout the annual cycle. Figure 9 shows the behavior of dry air (RH <20%) frequency at the 330 K isentropic level
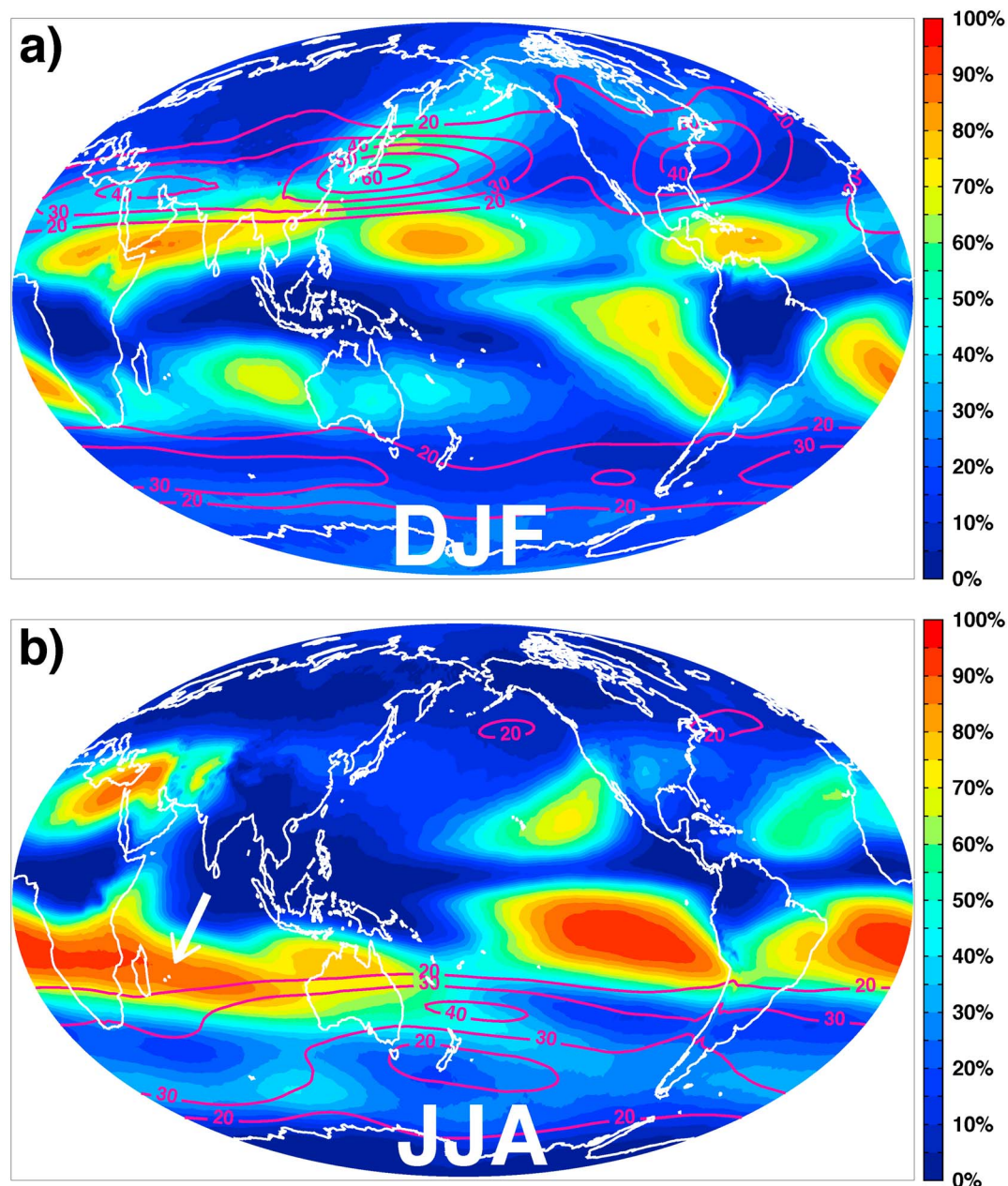
Figure 8. (a) Latitude-altitude cross section at 145°E of the occurrence frequency of dry air (RH <20%) during January–February 2014, derived from GFS analyses. Zonal winds, isentropes, and altitude of the PV = 2 tropopause (yellow line) are also included. (b) Cross section of water vapor mixing ratio at 145°E from GFS analysis.

calculated from averages over 2010–2014, for statistics during solstice seasons December-January-February (DJF) and June-July-August (JJA). The overall patterns show high occurrence frequency in the subtropics of both hemispheres, with relative maxima in the winter hemisphere. The corresponding patterns during the equinox seasons are similar overall (Figure S1 in the supporting information). In general, the maxima occur on the equatorward side of the strong subtropical jet streams. In the northern hemisphere (NH) winter (and spring; Figure S1) there are three frequency maxima which occur near the exit regions of the climatological jet maxima over the Middle East, the western Pacific, and North America. This co-location may suggest a relationship between the frequent occurrence of subtropical dry air and jet dynamics. The dry air is ubiquitous in the southern hemisphere (SH) subtropics during austral winter (JJA), with frequencies >90% over much of the globe except for the Australian-western Pacific sector. We have examined year-to-year variability in these patterns, and the large-scale features are repeatable for the most part each year (not shown).
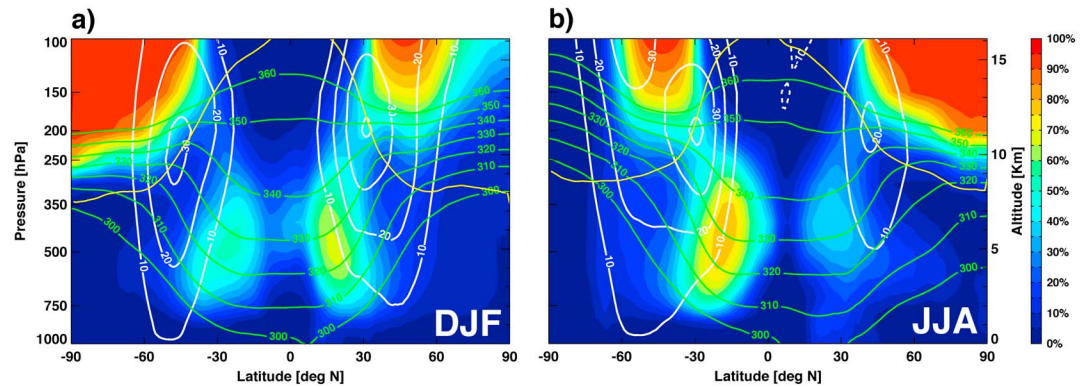
Latitude-height cross sections of the dry air occurrence frequency averaged over all longitudes during DJF and JJA are shown in Figure 10 to illustrate the behavior in relation to isentropes and jet structure. There are frequency maxima over ~10–30°N and ~10–30°S in both seasons on the equatorward side of the

Figure 9. Fractional occurrence of dry layers (RH <20%) on the 330 K isentrope during (a) DJF and (b) JJA, derived from GFS analyses over 2010–2014. The pink lines show the corresponding seasonal zonal winds. The white arrow in JJA denotes the location of Reunion Island.

subtropical jets, spanning isentropes ~310–340 K (altitudes 3–9 km). The maximum dry air frequency is larger in the winter hemisphere and more frequent in the SH compared to the NH (maximum frequency of ~75% in the SH during JJA versus ~60% in the NH during DJF, for the zonal average statistics in Figure 10). Similar patterns are observed for the equinox seasons (Figure S2), with more symmetry of the patterns between hemispheres.

The GFS data show that the subtropical dry air occurs most frequently in the winter hemisphere, linked with the strength of the subtropical jets. This behavior is illustrated in Figure 11, showing the zonal average occurrence frequency of RH <20% (derived from data points at all longitudes) at 330 K for the year 2014, together with the corresponding zonal average zonal winds. Dry air occurs frequently over 20–30°N and 20–30°S, with winter maxima on the equatorward side of the strongest subtropical jets. Frequent dry regions occur all year

Figure 10. Climatological (2010–2014) latitude-altitude cross sections of the occurrence frequency of dry air (RH <20%) calculated for all longitudes (i.e., zonal averages) during (a) DJF and (b) JJA. Zonal winds, isentropes, and altitude of the PV = 2 tropopause (yellow line) are also included.

in the SH, while in the NH there are relatively few during boreal summer. Close inspection of Figure 11 shows the high-frequency variations in the occurrence of dry layers, which may be linked to fluctuations in jet structure. Other years show similar overall behavior.
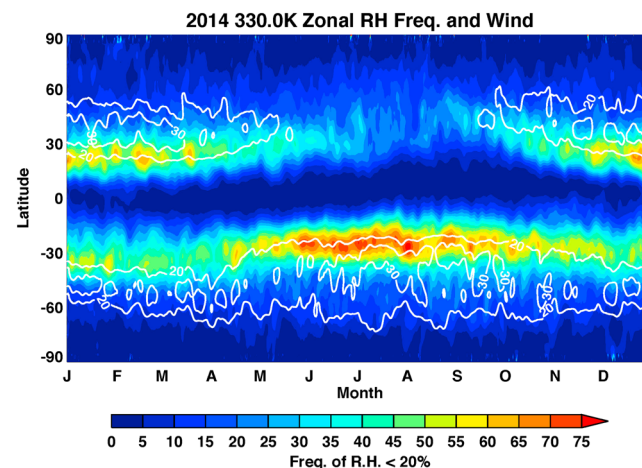
3.4. Water Vapor and Ozone Soundings from Reunion Island

The GFS data show that dry air is frequent in the SH subtropics during austral winter (Figures 9b and 11). It happens that the maximum occurrence frequency is located almost directly over Reunion Island (located with the arrow in Figure 9b), where long-term regular ozonesonde measurements have occurred [*Thompson et al.*, 2003; *Clain et al.*, 2009]. These data allow evaluation of humidity profiles (for comparison to GFS) and ozone-humidity relationships (for comparison to CONTRAST). Our analyses focus on measurements during June to August 1998–2015, including a total of ~170 soundings.

An example of the Reunion Island profile measurements is shown in Figure 12a. The ozone profile shows enhancements in the lower-middle troposphere (~3–8 km), coincident with dry air (RH <10%). The boundary layer is characterized by lower ozone and high RH, and ozone decreases above 8 km (before increasing to stratospheric values above 14 km). As noted above, the radiosonde RH measurements have larger uncertainties above 10 km and results are not analyzed above that level. The dry air (RH <20%) above the

Figure 11. Latitude versus month occurrence frequency of dry air (RH <20%) on the 330 K isentrope during 2014, derived from GFS analyses. Fractional values are calculated for each day using data at all longitudes (i.e., zonal averages). The white lines show the corresponding zonal average zonal winds at 330 K.
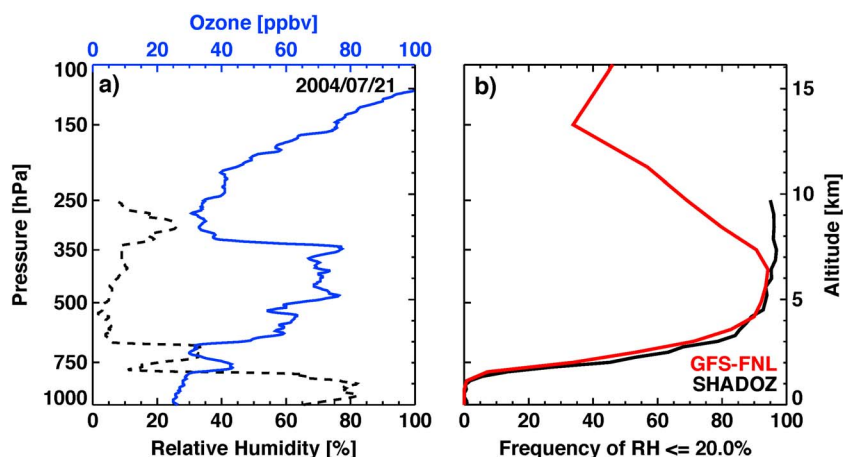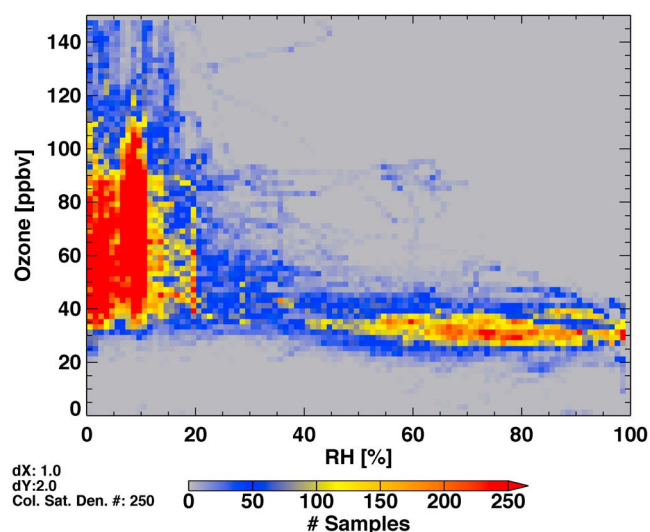
boundary layer is a frequent occurrence at Reunion Island during JJA, as shown in Figure 12b. The statistics derived from the balloon measurements agree well with results from the GFS analyses near Reunion (Figure 12b), with a clear maximum in occurrence for altitudes ~3–8 km (note that this is consistent with the behavior near 20°S in Figure 10).

The statistical relationship between ozone and RH derived from the Reunion soundings is shown in Figure 13, using all measurements over 0–10 km. These results show a bimodal distribution of air parcels with low RH (<20%) and enhanced ozone (~40–80 ppbv) versus those with low ozone (<40 ppbv) and RH >50%. The bimodal distribution is similar to the

Figure 12. (a) Vertical profiles of ozone and relative humidity (RH) from Reunion Island on 21 July 2004. (b) Frequency of occurrence of RH <20% derived from 170 Reunion Island ozonesonde profiles during JJA 1998–2015 (black) and GFS analyses at Reunion Island during JJA 2000–2014 (red). The radiosonde humidity measurements have large uncertainties above 10 km and are not shown.

CONTRAST statistics in Figure 3 and suggests a similar overall morphology and origin of the dry air for both situations. We note that frequently enhanced ozone in the troposphere (~6–10 km) at Reunion Island has been noted previously by *Baray et al.* [1998, 2000], who suggest an origin linked to persistent stratospheric air intrusions beneath the winter subtropical jet.

4. Summary and Discussion

Aircraft observations during CONTRAST detected the frequent occurrence of dry layers in the greater area around Guam (~0–20°N, 130–165°E). These layers occurred primarily over altitudes 3–9 km and were strongly correlated with enhanced ozone; the ozone-RH relationship (Figure 3) serves as a fingerprint of the distinct air characteristics. These dry, ozone-rich layers are similar to previous observations [*Newell et al.*, 1996; *Thouret et al.*, 2000], but the CONTRAST measurements showed much higher frequency and often much thicker layers than reported previously. These differences may be attributable to the location and timing of the CONTRAST

Figure 13. Two-dimensional distribution of ozone versus relative humidity for ozonesonde soundings at Reunion Island during JJA during 1998–2014 (total of 170 soundings). This distribution is based on measurements over 0–10 km.

observations, near a region of very frequent dry air (Figure 7). The relatively thick dry layers encountered during CONTRAST (e.g., RF02, RF06, and RF12 in Figure 4) may be linked to proximity to the subtropical jet, compared to measurements across a broad region of the tropics from PEM and MOZAIC; broader layers near the subtropical jets may be sheared by circulation into relatively narrow-scale features in the deep tropics. One objective of this paper was to compare the CONTRAST aircraft measurements of water vapor with results from GFS analysis. Our results show overall good agreement between the in situ measurements and global analyses, including for individual profile comparisons (Figures 4 and 5) and for the statistical behavior over the CONTRAST region (Figure 6). However, the lower vertical resolution of GFS does

not resolve the thinner layers, and GFS does not capture the driest layers. While the GFS analyses show a relative moist bias for the driest regions (Figure 5), the overall comparisons suggest that the analyses can accurately capture the magnitude and statistical behavior of dry air in the tropical and subtropical troposphere. This behavior is consistent with results based on ERA-40 reanalysis from *Cau et al.* [2005], and we have found similar good comparisons to CONTRAST measurements using ERA-Interim reanalysis (results not shown). The ability of the global analyses to capture the behavior of dry layers is likely attributable to assimilation of high vertical resolution water vapor measurements from satellite instruments such as AIRS [*Ruzmaikin et al.*, 2014] and IASI [e.g., *Hilton et al.*, 2009], combined with high-quality meteorological forecasts. *Rieckh et al.* [2016] have recently shown that retrievals from GPS radio occultation can also accurately capture the dry layer behavior.
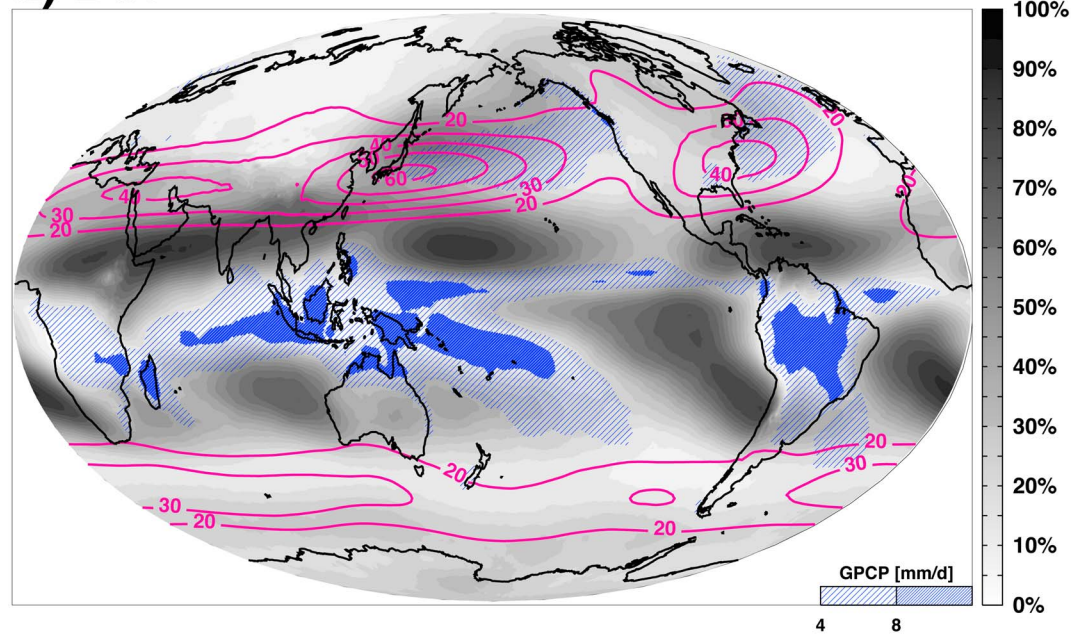
We have utilized the GFS analyses to quantify the frequency of occurrence and spatial structure of dry air during the time of the CONTRAST campaign. Dry air (RH $<20\%$) occurred frequently ($>70\%$) in the northern subtropics over longitudes ~60–180°E, on the equatorward side of the strong Asia-Pacific jet (Figure 7). This is precisely the region around Guam sampled by the CONTRAST measurements, so that CONTRAST was in the right location and right season to observe these features (although the goals of CONTRAST were mainly aimed at chemical behavior of the tropical upper troposphere, and the midtropospheric dry layers were not a prime objective). The GFS analyses show that subtropical dry air occurs primarily over potential temperature levels ~320–340 K (~3–9 km in the subtropics). These isentropes slope strongly upward with increasing latitude and intersect the extratropical UTLS (a reservoir of dry, ozone-rich air). The subtropical dry layers occur in the region of strong background gradients of water vapor (Figure 8b), which characterize the transition between tropical and extratropical air masses.

We have furthermore used the GFS analyses to characterize the climatological global behavior of dry air. The results (Figures 9–11 and S1 and S2) show dry air as a persistent feature of the subtropics throughout the year, with maximum occurrence on the equatorward side of the subtropical jets during the respective winter seasons. Our results are consistent with *Casey et al.* [2009], based on AIRS satellite data, although they focus mainly on the deep tropics and possible interactions of dry layers with convection (regions of outgoing longwave radiation $<240\,\mathrm{W\,m}^{-2}$). During NH winter (Figure 9a) the GFS data suggest three subtropical dry layer maxima, co-located with the downstream end of the subtropical jets over the Middle East, East Asia, and North America. Subtropical dry layers are especially ubiquitous in the SH winter (JJA), with occurrence frequencies $>80\%$ over most longitudes (aside from the southwest Pacific and over South America). In all seasons the subtropical dry air occurs primarily over isentropic levels ~320–340 K (Figure S2), consistent with the behavior observed in CONTRAST in situ measurements.
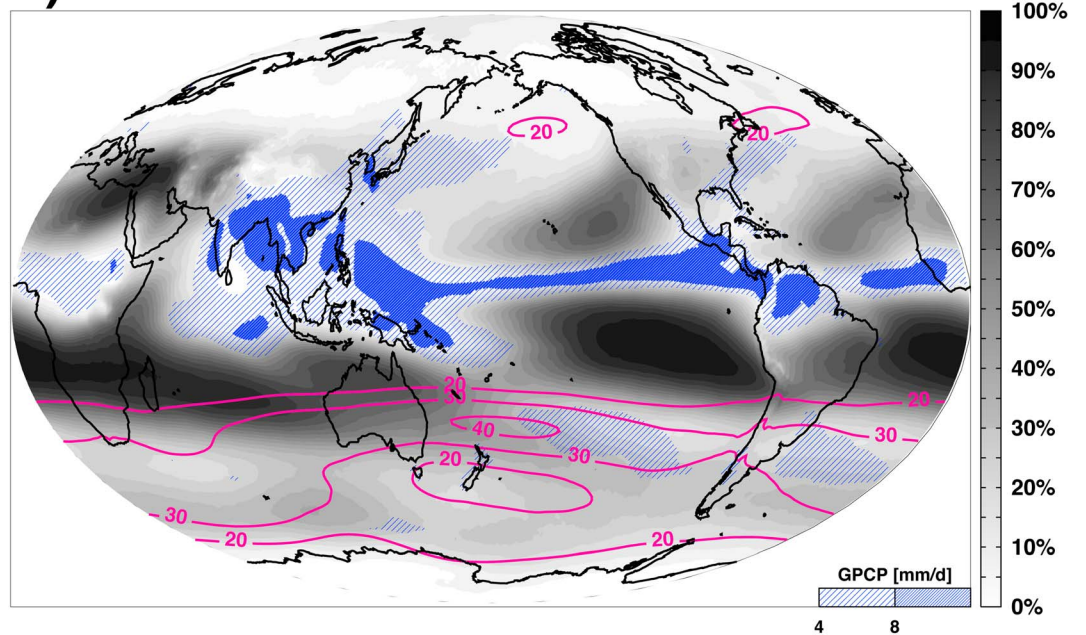
The climatological spatial patterns of the frequent dry air seen in Figure 9 can be partly explained by the location of climatological tropical precipitation, which will act to moisten, vertically homogenize, and remove dry layers. Figure 14 shows the dry air occurrence frequency during DJF and JJA (same data as in Figure 9), overlaid with climatological precipitation patterns derived from Global Precipitation Climatology Project [*Adler et al.*, 2003]. In both seasons the spatial patterns of frequent dry air and climatological precipitation are approximately orthogonal in the tropics, i.e., tropical regions that are distant from precipitation are characterized by frequent lower-middle tropospheric dry air. One interpretation of this behavior is that dry air can originate in the subtropics as a result of quasi-isentropic meridional transport [e.g., *Galewsky et al.*, 2005], and these layers are stable and can persist until encountering regions of persistent convection. Note that the large-scale patterns of tropical convection are forced by tropical circulations and low-level convergences; although the presence of midtropospheric dry layers may increase stability and tend to inhibit deep convection [e.g., *Mapes and Zuidema*, 1996; *Brown and Zhang*, 1997; *Parsons et al.*, 2000], they are probably not a dominant mechanism for setting the climatological precipitation structure.

The tropical precipitation and dry air patterns in Figure 14 are also closely linked with the local Hadley and Walker overturning circulations; regions of strong precipitation are linked with upward motions, while the dry layers occur in regions of climatological descent. The mean subsidence in the dry layer regions may help to suppress convection and lead to overall drying in these regions. However, the characteristic signatures of horizontally layered dry structures, correlated with high ozone, occurring primarily over isentropic layers connecting the subtropical troposphere to the extratropical UTLS, are most simply explained by persistent quasi-
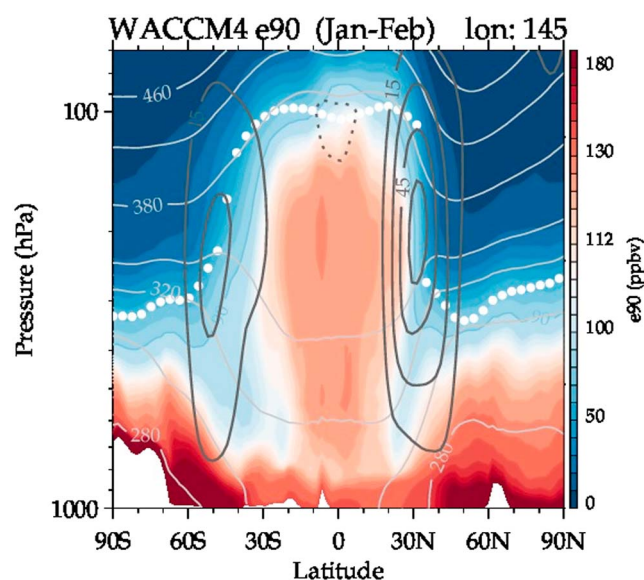
Figure 14. Distribution of dry layer occurrence frequency at the 330 K isentropic level (grey scale), overlain with climatological precipitation derived from GPCP (blue colors). Results are shown for (a) DJF and (b) JJA. The pink lines denote the seasonal zonal winds (m/s) at 330 K.

isentropic mixing under the core of the subtropical jet (linked to Rossby waves, persistent large-scale tropopause folds [*Baray et al.*, 2000], or the variety of dynamical mechanisms discussed by *Cau et al.* [2007]). This interpretation is consistent with the water vapor trajectory studies of *Galewsky et al.* [2005] and *Cau et al.* [2007] and with the well-known behavior of quasi-isentropic mixing between low and middle latitudes [e.g., *Pierrehumbert and Yang*, 1993; *Bowman and Carrie*, 2002]. We note that this layered behavior occurs primarily below the subtropical jet core, and is consistent with the weaker transport across the jet core [*Haynes and Shuckburgh*, 2000; *Abalos et al.*, 2016], which provides a simple explanation for why the

Figure 15. Meridional cross section of the idealized tracer e90, derived from a WACCM simulation using nudged meteorology (details discussed in text). This cross section is for a longitude near Guam (145°E) for statistics over January–February 2014. The background includes the time average zonal winds, isentropes, and the thermal tropopause (white dots). Figure courtesy of Mijeong Park and Doug Kinnison.

subtropical dry air does not typically extend above ~9 km (340 K; i.e., this process sets the vertical scale of the dry layers). Such behavior would not be expected as a result of tropical subsidence.

The strong correlation of enhanced ozone with dry subtropical air is a key signature of an origin in the extratropical UTLS. This behavior is observed in CONTRAST aircraft measurements (Figure 3) and also in water vapor and ozone soundings from Reunion Island (Figure 13), which is located near the maximum dry air frequency in the SH subtropics identified in GFS data. The Reunion Island balloon observations show frequent dry air in the lower-middle troposphere, in excellent agreement with GFS statistics (Figure 12b). Furthermore, the distribution of ozone versus RH at Reunion Island (Figure 13) shows strong evidence for a bimodal distribution, similar to the CONTRAST statistics (Figure 3). We view the ozone-RH behavior as a fingerprint to identify the surprisingly important extratropical UTLS influence on tropical and subtropical tropospheric air. As a note, *Zhang et al.* [2003] have documented a bimodal behavior of tropical tropospheric water vapor, similar to the statistical results shown here.

We note that the signatures of subtropical dry air discussed here, and proposed links to the extratropical UTLS, are consistent with the behavior of the tracer e90 discussed in *Prather et al.* [2011]. e90 is an idealized model tracer with origin at the surface and a 90 day decay time, which identifies tropospheric and stratospheric air masses and the location of the tropopause. *Prather et al.* [2011] use e90 to show that the oldest air in the tropical troposphere in their model occurs in the winter subtropics, with similar distribution to the dry air statistics identified here. We have examined the tracer e90 as simulated in the Whole Atmosphere Community Climate Model chemistry-climate model using meteorological fields nudged to analyses [*Lamarque et al.*, 2012], and Figure 15 shows a cross section of e90 in the western Pacific (near the longitude of Guam) for January–February 2014. These patterns show tongues of relatively small e90 (i.e., relatively aged air) extending along isentropes from the extratropical UTLS region into the subtropical troposphere in both hemispheres (similar to the dry air statistics in Figure 8a). This behavior is consistent with the model results in *Prather et al.* [2011], and the morphology of this idealized tracer supports our interpretation of a UTLS origin for the dry, ozone-enhanced subtropical layers.

One quantitative aspect of the dry, high-ozone layers is that while the associated ozone values are clearly above background levels for the troposphere (~20–30 ppbv), the enhanced ozone amounts (~40–70 ppbv for CONTRAST and ~40–90 ppbv for Reunion Island) are far from "stratospheric" (hundreds of parts per billion by volume, with a value of ~80–100 ppbv typically chosen as a definition of a stratospheric value [*Bethan et al.*, 1996; *Prather et al.*, 2011]). This behavior could result from mixing or dilution during isentropic transport from the extratropical UTLS, although the details of such mixing are poorly understood. Likewise, the spatial extent and ozone amounts of the background UTLS reservoir region inferred in our results are not well constrained.

Anderson et al. [2016] have provided a somewhat different interpretation of the high-ozone/low-water structures observed in CONTRAST, arguing for a strong influence of biomass burning (as a source of enhanced ozone) tied to large-scale subsidence (as a source of dry air). While biomass burning may indeed contribute

to tropical tropospheric ozone formation [e.g., *Kondo et al.*, 2004], there are several points of evidence to suggest that subsidence is not the primary cause of the ubiquitous dry layers. These include their horizontally layered behavior (Figure 1), most frequent occurrence for isentropes ~320–340 K (and not above), and trajectory-based calculations [e.g., *Galewsky et al.*, 2005; *Cau et al.*, 2007], demonstrating the dominance of isentropic transport from the extratropical UTLS. Furthermore, the balloon observations from Reunion Island demonstrate that enhanced ozone is a pervasive feature of the subtropical dry layers; note that while biomass burning from Africa may influence Reunion Island during austral spring (maximum during October–November [*Clain et al.*, 2009]), the dry layers (with enhanced ozone) occur primarily during winter (JJA), when the subtropical jet is strongest and closest to Reunion Island. Overall, while biomass burning may impact tropical ozone, its seasonal and episodic behavior does not support the ubiquitous occurrence of dry layers correlated with enhanced ozone in the subtropics. The 3-D structure of dry layer occurrence, links to the subtropical jets (in both hemispheres), observed seasonal variations, and close links to enhanced ozone; all argue for a primary source region in the extratropical UTLS (as a reservoir of dry, ozone-rich air).

References

Abalos, M., B. Legras, and E. Shuckburgh (2016), Interannual variability in effective diffusivity in the upper troposphere/lower stratosphere from reanalysis data, *Q. J. R. Meteorol. Soc.*, *142*, 1847–1861, doi:10.1002/qj.2779.

Adler, R. F., et al. (2003), The version-2 Global Precipitation Climatology Project (GPCP) monthly precipitation analysis (1979–present), *J. Hydrometeorol.*, *4*, 1147–1167.

Anderson, D. C., et al. (2016), A pervasive role for biomass burning in tropical high ozone/low water structures, *Nat. Comm.*, *7*, doi:10.1038/ncomms10267.

Baray, J. L., G. Ancellet, F. G. Taupin, M. Bessafi, S. Baldy, and P. Keckhut (1998), Subtropical tropopause break as a possible stratospheric source of ozone in the tropical troposphere, *J. Atmos. Sol. Terr. Phys.*, *60*, 27–36.

Baray, J. L., V. Daniel, G. Ancellet, and B. Legras (2000), Planetary-scale tropopause folds in the southern subtropics, *Geophys. Res. Lett.*, *27*, 353–356, doi:10.1029/1999GL010788.

Bethan, S., G. Vaughan, and S. Reid (1996), A comparison of ozone and thermal tropopause heights and the impact of tropopause definition on quantifying the ozone content of the troposphere, *Q. J. R. Meteorol. Soc.*, *122*, 929–944.

Birner, T., S. M. Davis, and D. J. Seidel (2014), The changing width of Earth's tropical belt, *Phys. Today*, *67*(12), 38–44.

Bowman, K. P., and G. D. Carrie (2002), The mean-meridional transport circulation of the troposphere in an idealized GCM, *J. Atmos. Sci.*, *59*, 1502–1514.

Brown, R. G., and C. Zhang (1997), Variability of midtropospheric moisture and its effect on cloud-top height distribution during TOGA COARE, *J. Atmos. Sci.*, *54*, 2760–2774.

Casey, S. P. F., A. E. Dessler, and C. Schumacher (2009), Five-year climatology of midtroposphere dry air layers in warm tropical ocean regions as viewed by AIRS/Aqua, *J. Appl. Meteorol. Climatol.*, *48*, 1831–1842, doi:10.1175/2009JAMC2099.1.

Cau, P., J. Methven, and B. Hoskins (2005), Representation of dry tropical layers and their origins in ERA-40 data, *J. Geophys. Res.*, *110*, D06110, doi:10.1029/2004JD004928.

Cau, P., J. Methven, and B. Hoskins (2007), Origins of dry air in the tropics and subtropics, *J. Clim.*, *20*, 2745–2759.

Ciesielski, P. E., et al. (2014), Quality-controlled upper-air sounding dataset for DYNAMO/CINDY/AMIE: Development and corrections, *J. Atmos. Oceanic Technol.*, *31*, 741–764.

Clain, G., J. L. Baray, R. Delmas, R. Diab, J. Leclair de Bellevue, P. Keckhut, F. Posny, J. M. Metzger, and J. P. Cammas (2009), Tropospheric ozone climatology at two Southern Hemisphere tropical/subtropical sites, (Reunion Island and Irene, South Africa) from ozonesondes, lidar, and in situ aircraft measurements, *Atmos. Chem. Phys.*, *9*, 1723–1734. [Available at www.atmos-chem-phys.net/9/1723/2009/.]

Dessler, A. E., and K. Minschwaner (2007), An analysis of the regulation of tropical tropospheric water vapor, *J. Geophys. Res.*, *112*, D10120, doi:10.1029/2006JD007683.

Galewsky, J., A. Sobel, and I. Held (2005), Diagnosis of subtropical humidity dynamics using tracers of last saturation, *J. Atmos. Sci.*, *62*, 3353–3367.

Gettelman, A., W. D. Collins, E. J. Fetzer, A. Eldering, F. W. Irion, P. B. Duffy, and G. Bala (2006), Climatology of upper tropospheric relative humidity from the atmospheric infrared sounder and implications for climate, *J. Clim.*, *19*(23), 6104–6121.

Hayashi, H., K. Kita, and S. Taguchi (2008), Ozone-enhanced layers in the troposphere over the equatorial Pacific Ocean and the influence of transport of midlatitude UT/LS air, *Atmos. Chem. Phys.*, *8*, 2609–2621, doi:10.5194/acp-8-2609-2008.

Haynes, P., and E. Shuckburgh (2000), Effective diffusivity as a diagnostic of atmospheric transport: 2. Troposphere and lower stratosphere, *J. Geophys. Res.*, *105*, 22,795–22,810, doi:10.1029/2000JD900092.

Hilton, F., N. C. Atkinson, S. J. English, and J. R. Eyre (2009), Assimilation of IASI at the Met Office and assessment of its impact through observing system experiments, *Q. J. R. Meteorol. Soc.*, *135*, 495–505, doi:10.1002/qj.379.

Kley, D., H. G. J. Smit, H. Vömel, H. Grassl, V. Ramanathan, P. J. Crutzen, S. Williams, J. Meywerk, and S. J. Oltmans (1997), Tropospheric water-vapour and ozone cross-sections in a zonal plane over the central equatorial Pacific Ocean, *Q. J. R. Meteorol. Soc.*, *123*, 2009–2040.

Kley, D., H. G. J. Smit, S. Nawrath, Z. Luo, P. Nedelec, and R. H. Johnson (2007), Tropical Atlantic convection as revealed by ozone and relative humidity measurements, *J. Geophys. Res.*, *112*, D23109, doi:10.1029/2007JD008599.

Kondo, Y., et al. (2004), Impacts of biomass burning in Southeast Asia on ozone and reactive nitrogen over the western Pacific in spring, *J. Geophys. Res.*, *109*, D15S12, doi:10.1029/2003JD004203.

Lamarque, J. F., et al. (2012), CAM-chem: Description and evaluation of interactive atmospheric chemistry in the Community Earth System Model, *Geosci. Model Dev.*, *5*, 369–411, doi:10.5194/gmd-5-369-2012.

Mapes, B., and P. Zuidema (1996), Radiative-dynamical consequences of dry tongues in the tropical troposphere, *J. Atmos. Sci.*, *53*, 620–638.

Miloshevich, L. M., H. Vomel, D. N. Whiteman, B. M. Lesht, F. J. Schmidlin, and F. Russo (2006), Absolute accuracy of water vapor measurements from six operational radiosonde types launched during AWEX-G and implications for AIRS validation, *J. Geophys. Res.*, *111*, D09S10, doi:10.1029/2005JD006083.

Newell, R. E., Z.-X. Wu, Y. Zhu, W. Hu, E. V. Browell, G. L. Gregory, G. W. Sachse, J. E. Collins Jr., K. K. Kelly, and S. C. Liu (1996), Vertical fine-scale atmospheric structure measured from NASA DC-8 during PEM-West A, *J. Geophys. Res.*, *101*, 1943–1960, doi:10.1029/95JD02613.

Newell, R. E., V. Thouret, J. Y. N. Cho, P. Stoller, A. Marenco, and H. G. Smit (1999), Ubiquity of quasi-horizontal layers in the troposphere, *Nature*, *398*, 316–319.

Pan, L. L., et al. (2015), Bimodal distribution of free tropospheric ozone over the tropical western Pacific revealed by airborne observations, *Geophys. Res. Lett.*, *42*, 7844–7851, doi:10.1002/2015GL065562.

Pan, L. L., et al. (2016), The Convective Transport of Active Species in the Tropics (CONTRAST) experiment, *Bull. Am. Meteorol. Soc.*, doi:10.1175/BAMS-D-14-00272.1, in press.

Parsons, D. B., K. Yoneyama, and J.-L. Redelsperger (2000), The evolution of the tropical western Pacific atmosphere-ocean system following the arrival of a dry intrusion, *Q. J. R. Meteorol. Soc.*, *126*, 517–548.

Pierrehumbert, R. T. (1995), Thermostats, radiator fins, and the local runaway greenhouse, *J. Atmos. Sci.*, *52*, 1784–1806.

Pierrehumbert, R. T., and H. Yang (1993), Global chaotic mixing on isentropic surfaces, *J. Atmos. Sci.*, *50*, 2462–2480.

Prather, M. J., X. Zhu, Q. Tang, J. Hsu, and J. L. Neu (2011), An atmospheric chemist in search of the tropopause, *J. Geophys. Res.*, *116*, D04306, doi:10.1029/2010JD014939.

Ridley, B. A., F. E. Grahek, and J. G. Walega (1992), A small, high-sensitivity, medium-response ozone detector for measurements from light aircraft, *J. Atmos. Oceanic Technol.*, *9*, 142–148.

Rieckh, T., R. Anthes, W. J. Randel, S.-P. Ho, and U. Foelsche (2016), Tropospheric dry layers in the tropical western Pacific: Comparisons of GPS radio occultation with multiple data sets, *Atmos. Meas. Tech. Discuss.*, doi:10.5194/amt-2016-258.

Ruzmaikin, A., H. H. Aumann, and E. M. Manning (2014), Relative humidity in the troposphere with AIRS, *J. Atmos. Sci.*, *71*, 2516–2533.

Sherwood, S. C., R. Roca, T. M. Weckwerth, and N. G. Andronova (2009), Tropospheric water vapor, convection, and climate, *Rev. Geophys.*, *48*, RG2001, doi:10.1029/2009RG000301.

Smit, H. G. J., et al. (2007), Assessment of the performance of ECC-ozonesondes under quasi-flight conditions in the environmental simulation chamber: Insights from the Juelich Ozone Sonde Intercomparison Experiment (JOSIE), *J. Geophys. Res.*, *112*, D19306, doi:10.1029/2006JD007308.

Stoller, P., et al. (1999), Measurements of atmospheric layers from the NASA DC-8 and P-3B aircraft during PEM-Tropics A, *J. Geophys. Res.*, *104*, 5745–5764, doi:10.1029/98JD02717.

Thompson, A. M., et al. (2003), Southern Hemisphere Additional Ozonesondes (SHADOZ) 1998–2000 tropical ozone climatology, 1, Comparison with Total Ozone Mapping Spectrometer (TOMS) and ground-based measurements, *J. Geophys. Res.*, *108*(D2), 8238, doi:10.1029/2001JD000967.

Thouret, V., J. Y. N. Cho, R. E. Newell, A. Marenco, and H. G. J. Smit (2000), General characteristics of tropospheric trace constituent layers observed in the MOZAIC program, *J. Geophys. Res.*, *105*, 17,379–17,392, doi:10.1029/2000JD900238.

Thouret, V., J. Y. N. Cho, M. J. Evans, R. E. Newell, M. A. Avery, J. D. W. Barrick, G. W. Sachse, and G. L. Gregory (2001), Tropospheric ozone layers observed during PEM-Tropics B, *J. Geophys. Res.*, *106*, 32,527–32,538, doi:10.1029/2001JD900011.

Wu, Z.-X., R. E. Newell, Y. Zhu, B. E. Anderson, E. V. Browell, G. L. Gregory, G. W. Sachse, and J. E. Collins Jr. (1997), Atmospheric layers measured from the NASA DC-8 during PEM-West B and comparison with PEM-West A, *J. Geophys. Res.*, *102*, 28,353–28,365, doi:10.1029/97JD01097.

Yoneyama, K., and D. B. Parsons (1999), A proposed mechanism for the intrusion of dry air into the tropical western Pacific region, *J. Atmos. Sci.*, *56*, 1524–1546.

Zhang, C., B. E. Mapes, and B. J. Soden (2003), Bimodality in tropical water vapour, *Q. J. R. Meteorol. Soc.*, *129*, 2847–2866.

Zondlo, M. A., M. E. Paige, S. M. Massick, and J. A. Silver (2010), Development, flight performance, and calibrations of the NSF Gulfstream-V vertical cavity surface emitting laser (VCSEL) hygrometer, *J. Geophys. Res.*, *115*, D20309, doi:10.1029/2010JD014445.

Erratum

In the originally published version of this article, the Acknowledgments section was incomplete. The sentence has been added: "We acknowledge the support of Bernard Legras, Pasquale Sellitto, and the department of Geosciences at Ecole Normale Supérieure, Paris, institution to which co-author Louis Rivoire was affiliated during the research project." This version may be considered the authoritative version of record.